Supporting Information for:

Controlling Nd-to-Yb Energy Transfer through a Molecular Approach

Flavia Artizzu,[*,a,b] Angela Serpe, Luciano Marchiò,[c] Michele Saba,[a] Andrea Mura,[a] Maria Laura Mercuri,[b] Giovanni Bongiovanni,[a] Paola Deplano,*[*,a,b] and Francesco Quochi.*[*,a]*

[a]Dipartimento di Fisica and [b]Dipartimento di Scienze Chimiche e Geologiche, Università di Cagliari, Complesso Universitario di Monserrato, I-09042 Monserrato-Cagliari, Italy

[c]Dipartimento di Chimica, Università di Parma, Parco Area delle Scienze 17A, I-43100 Parma, Italy

AUTHOR INFORMATION

Corresponding Author

*Flavia Artizzu, f.artizzu@unica.it.

*Paola Deplano, deplano@unica.it

*Francesco Quochi, francesco.quochi@dsf.unica.it.

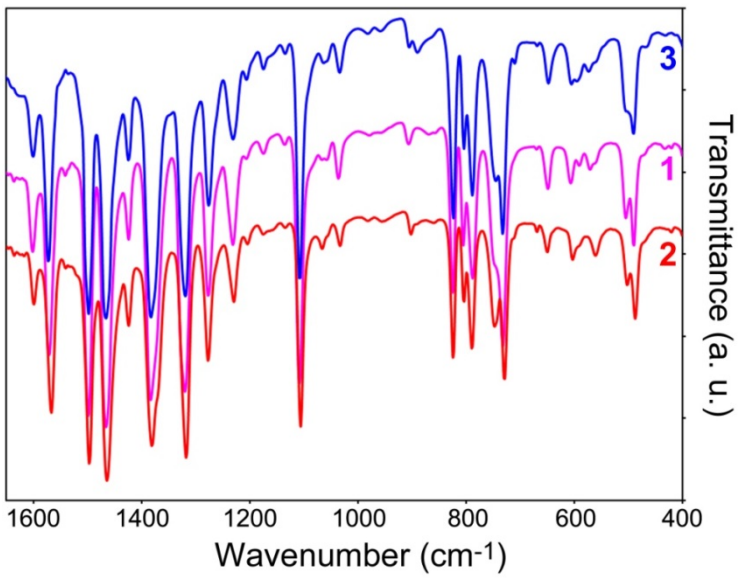

Figure S1. FT-IR spectra of compounds **1**-**3** in the 1600-400 cm^{-1} range. All spectra display the typical fingerprints of a trinuclear quinolinolate complex of general formula Ln_3Q_9,[10] and are mainly dominated by the aromatic ring vibrations of the Q ligand with only slight modifications due to coordination. As expected, the bands below 800 cm^{-1} seem to be somewhat sensitive to the coordinated metal and are slightly shifted to lower wavenumbers as the weight of the coordinated lanthanide ion decreases (Yb *vs* Nd). Likewise, the band near 1100 cm^{-1}, assigned to the stretching vibration of the coordinating C–O, is affected to some extent by the weight of the metal. The corresponding bands for **1** appear slightly broadened and at intermediate wavenumbers with respect to **2** and **3**. See Experimental Section for details.

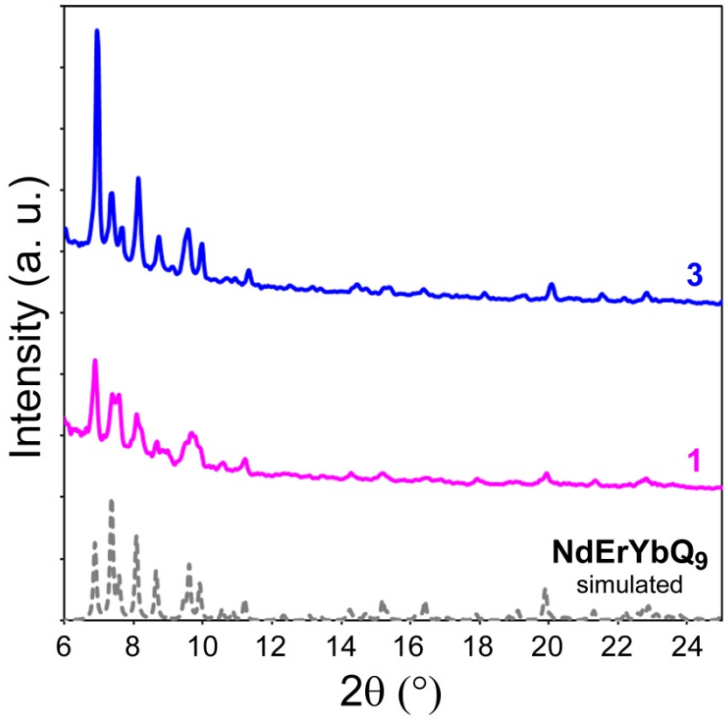

Figure S2. Experimental powder-XRD patterns of **1** (purple) and **3** (blue), in the 6-25° angle (2θ) range, and comparison with the powder diffractogram of the heterolanthanide trinuclear $NdErYbQ_9$ complex[12] simulated from single crystal X-ray diffraction data. Differences in peaks intensities are related to preferential orientations.

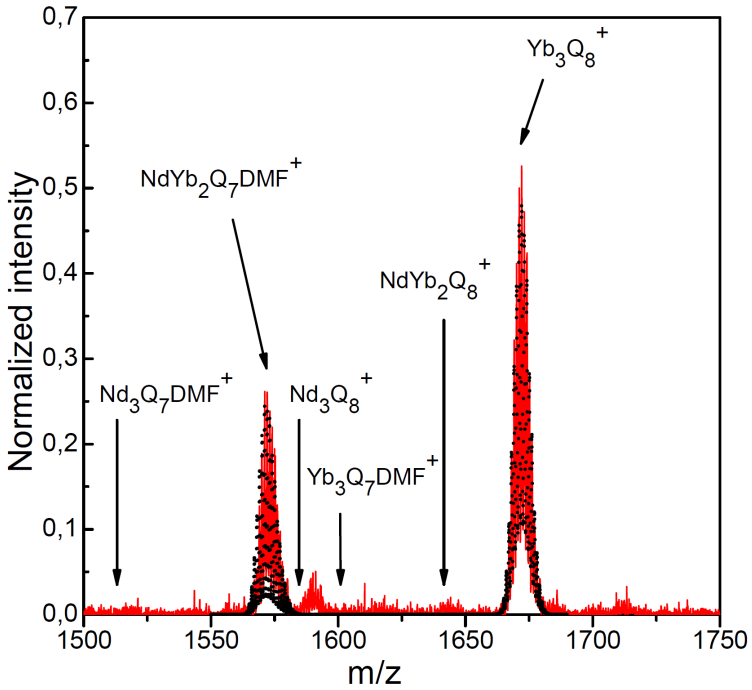

Figure S3. ESI-mass spectrum of **1** in the 1500-1750 m/z region. Predicted positions of possible molecular fragments are indicated.

Molecular speciation for 1

Model a: $\boldsymbol{a_m NdYb_2Q_9 + a_{Yb} Yb_3Q_9}$

Number of Yb ions: $N_{\mathrm{Yb}} = 2a_m + 3a_{\mathrm{Yb}}$

Number of Nd ions: $N_{\mathrm{Nd}} = a_m$

ICP-mass experiment: $N_{\mathrm{Yb}} = 2.07;\ N_{\mathrm{Nd}} = 0.93$

Ion-number ratio: $\frac{N_{\mathrm{Yb}}}{N_{\mathrm{Nd}}} = \frac{2a_m+3a_{Yb}}{a_m} \rightarrow \frac{a_{\mathrm{Yb}}}{a_m} = \frac{1}{3}\left(\frac{N_{\mathrm{Yb}}}{N_{\mathrm{Nd}}} - 2\right)$

$NdYb_2Q_9$ molar fraction: $\eta_m = \frac{a_m}{a_{\mathrm{Yb}}+a_m} = \frac{1}{1+\frac{a_{\mathrm{Yb}}}{a_m}}$

Yb_3Q_9 molar fraction: $\eta_{\mathrm{Yb}} = \frac{a_{\mathrm{Yb}}}{a_{\mathrm{Yb}}+a_m} = \frac{1}{1+\left(\frac{a_{\mathrm{Yb}}}{a_m}\right)^{-1}}$

Model b: $\boldsymbol{a_{Nd} Nd_3Q_9 + a_m NdYb_2Q_9 + a_{Yb} Yb_3Q_9}$

Nd_3Q_9 molar fraction: $\eta_{\mathrm{Nd}} = \frac{a_{\mathrm{Nd}}}{a_{\mathrm{Nd}}+a_m+a_{\mathrm{Yb}}} = \frac{1}{1+a_m^{'}+a_{\mathrm{Yb}}^{'}}$

where $a_m^{'} = \frac{a_m}{a_{\mathrm{Nd}}}$ and $a_{\mathrm{Yb}}^{'} = \frac{a_{\mathrm{Yb}}}{a_{\mathrm{Nd}}}$;

$\rightarrow a_m^{'} = \eta_{\mathrm{Nd}}^{-1} - a_{\mathrm{Yb}}^{'} - 1$ **(1)**

Transient NIR-PL spectroscopy exp.: $\eta_{\mathrm{Nd}} = 0.13(1)$

Number of Nd ions: $N_{\mathrm{Nd}} = 3a_{\mathrm{Nd}} + a_m$

Number of Yb ions: $N_{\mathrm{Yb}} = 2a_m + 3a_{\mathrm{Yb}}$

ICP-mass experiment: $N_{\mathrm{Yb}} = 2.07;\ N_{\mathrm{Nd}} = 0.93$

Ion-number ratio: $\frac{N_{\mathrm{Yb}}}{N_{\mathrm{Nd}}} = \frac{2a_m+3a_{\mathrm{Yb}}}{3a_{\mathrm{Nd}}+a_m} \rightarrow \frac{2a_m^{'}+3a_{\mathrm{Yb}}^{'}}{3+a_m^{'}} = \frac{N_{\mathrm{Yb}}}{N_{\mathrm{Nd}}}$ **(2)**

Combining Eqs. **(1)** and **(2)**: $a_{\mathrm{Yb}}^{'} = \left[2\left(1-\eta_{\mathrm{Nd}}^{-1}\right) + \frac{N_{\mathrm{Yb}}}{N_{\mathrm{Nd}}}\left(2+\eta_{\mathrm{Nd}}^{-1}\right)\right] / \left(1+\frac{N_{\mathrm{Yb}}}{N_{\mathrm{Nd}}}\right)$

$NdYb_2Q_9$ molar fraction: $\eta_m = \frac{a_m}{a_{\mathrm{Nd}}+a_m+a_{\mathrm{Yb}}} = \frac{a_m^{'}}{1+a_m^{'}+a_{\mathrm{Yb}}^{'}}$

Yb_3Q_9 molar fraction: $\eta_{\mathrm{Yb}} = \frac{a_{\mathrm{Yb}}}{a_{\mathrm{Nd}}+a_m+a_{\mathrm{Yb}}} = \frac{a_{\mathrm{Yb}}^{'}}{1+a_m^{'}+a_{\mathrm{Yb}}^{'}}$

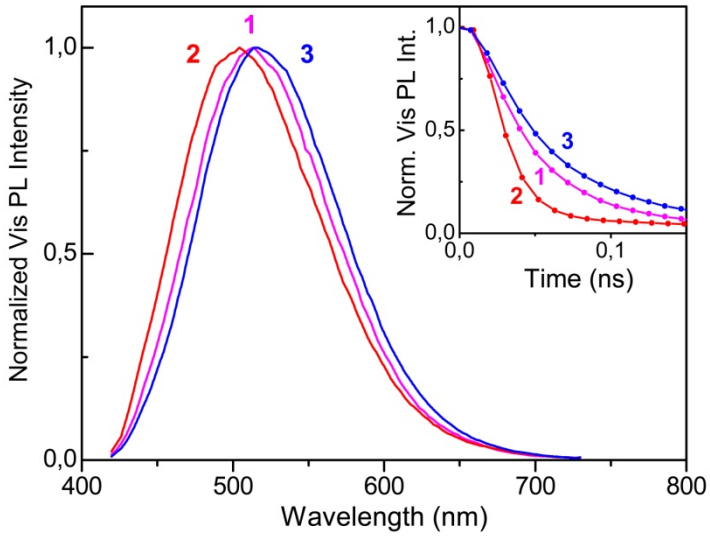

Figure S4. Q ligand residual fluorescence in the visible region for **1-3** under irradiation at 355 nm. Time-resolved decay dynamics is shown in the inset.

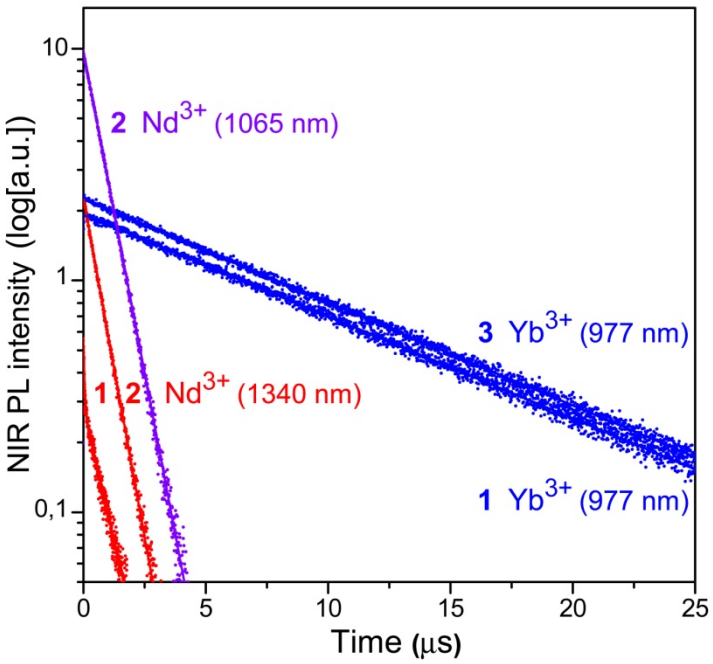

Figure S5. Time resolved PL for **1-3** in the NIR region: Yb^{3+} $^2F_{5/2} \rightarrow {}^2F_{3/2}$ decay at 977 nm (blue), Nd^{3+} $^4F_{3/2} \rightarrow {}^4I_{13/2}$ decay at 1340 nm (red) and Nd^{3+} $^4F_{3/2} \rightarrow {}^4I_{11/2}$ decay at 1065 nm (purple). In **2**, transitions giving rise to emission at 1065 and 1340 nm (and 890 nm, not shown for clarity) share the same starting level, therefore the observed decay dynamics is independent of the monitored wavelength.

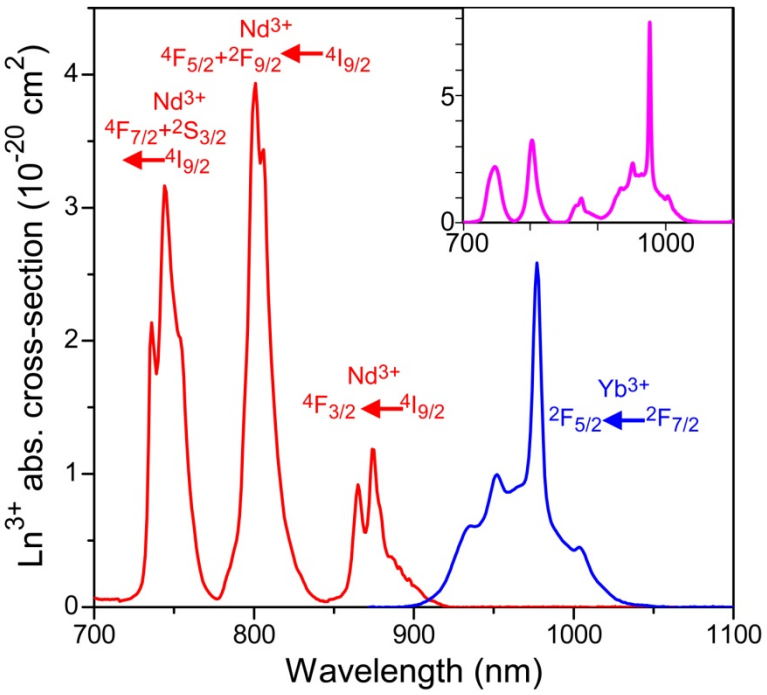

Figure S6. Absorption cross-sections of Nd^{3+} (red) and Yb^{3+} (blue) for **2** and **3** in DMSO solution in the 700-1100 nm region, appropriately normalized to a single metal ion. In the inset the experimental absorption cross-section of **1** in DMSO solution is reported.

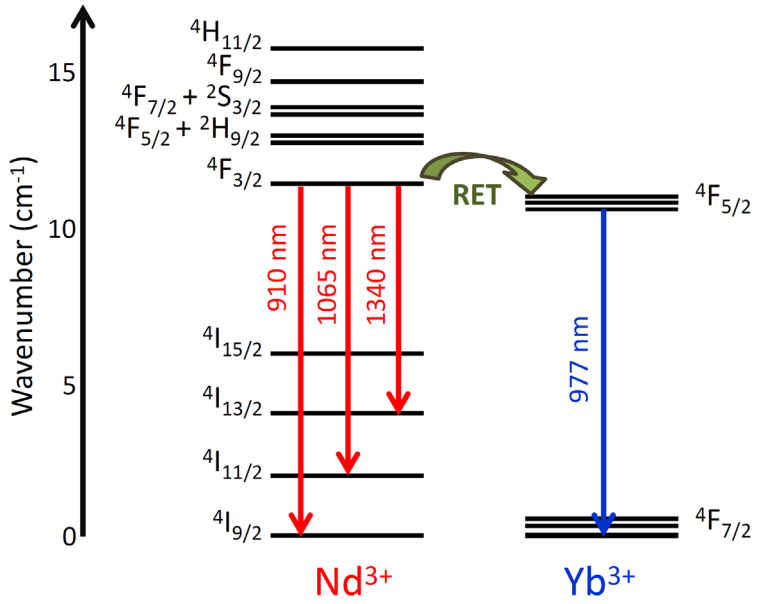

Figure S7. Energy level diagram for Nd^{3+} and Yb^{3+}. Radiative transitions and non-radiative energy transfer process are indicated.

NIR-PL temporal dynamics

Fit model function for Nd dynamics in **1**

$$I_{\mathrm{Nd}}(t) = A_{\mathrm{Nd}} \exp(-t/\tau_{\mathrm{Nd}}) + A^*_{\mathrm{Nd}} \exp(-t/\tau^*_{\mathrm{Nd}}) \qquad \text{Eq. S1}$$

where A_{Nd} is the amplitude of the Nd^{3+} signal (at 1350 nm) in Nd_3Q_9, A^*_{Nd} is the amplitude of Nd^{3+} signal in $NdYb_2Q_9$, τ_{Nd} is the Nd^{3+} excited-state decay time in Nd_3Q_9 (absence of Yb^{3+} acceptor), and τ^*_{Nd} is the Nd^{3+} excited-state decay time in $NdYb_2Q_9$ (presence of Yb^{3+} acceptor)

Fit model functions for Yb dynamics (Figure 4)

$$I_{\mathrm{Yb}}(t) = A_{\mathrm{Yb}} \exp(-t/\tau_{\mathrm{Yb}}) + A^*_{\mathrm{Yb}} \exp(-t/\tau_{\mathrm{Yb}})[1 - \exp(-t/\tau^*_{\mathrm{Yb}} + t/\tau_{\mathrm{Yb}})] \qquad \text{Eq. S2}$$

$$I_{\mathrm{Yb,eq}}(t) = A_{\mathrm{Yb,eq}} \exp(-t/\tau_{\mathrm{Yb}}) \qquad \text{Eq. S3}$$

I_{Yb} is the intensity of Yb^{3+} signal (at 977 nm) in $NdYb_2Q_9$ molecules in **1**. A_{Yb} is the amplitude of the Yb^{3+} signal related to ions directly sensitized by the photoexcited Q ligand, A^*_{Yb} is the amplitude of the Yb^{3+} signal due to Nd-to-Yb energy transfer, τ_{Yb} is the Yb^{3+} excited-state decay time, and τ^*_{Yb} is the Yb^{3+} activation time constant. $I_{\mathrm{Yb,eq}}$ is the predicted intensity for a quantity of Yb_3Q_9 substance equal to the measured quantity of $NdYb_2Q_9$, and $A_{\mathrm{Yb,eq}}$ is its amplitude.

Table S1. Fit values of transient NIR PL parameters for **1**-**3**.

Lifetimes (μs)

	$\tau_{Nd}{}^*$	τ_{Nd}	$\tau_{Yb}{}^*$	τ_{Yb}
1	0.044(1)	0.95(1)	0.035(1)	9.86(1)
2		0.74(1)		
3				9.76(1)

Amplitudes (mV± 2%)

	$A_{Nd}{}^*$	A_{Nd}	$A_{Yb}{}^*$	A_{Yb}
1	0.283	0.282	0.245	1.68
2		2.27		
3				2.24

Nd-to-Yb and Yb-to-Nd Förster's energy transfer

D = donor; A = acceptor

$J = \int F_{\mathrm{D}}(\lambda)\sigma_{\mathrm{A}}(\lambda)\lambda^4 d\lambda$ Spectral overlap integral

$F_D(\lambda)$ Donor emission spectral density

$\sigma_A(\lambda)$ Acceptor absorption cross-section

$R_0 = \sqrt[6]{\frac{9\kappa_j^2}{128\pi^5 n^4}J}$ Förster's radius

$\kappa^2 = 0.667$ Geometrical parameter

$n = 1.478$ Refractive index for DMSO

$\kappa_{\mathrm{ET}} = \frac{1}{\tau_{\mathrm{ET}}} = \frac{1}{\tau_{\mathrm{D}}}\left(\frac{R_0}{R_{\mathrm{DA}}}\right)^6$ Energy transfer rate constant

$R_{DA} = 0.36$ nm Donor-acceptor distance

τ_D Decay time constant of the donor in the absence of the acceptor

Table S2. Förster's parameters for Nd-Yb ET and energy back transfer in **1**.

	τ_D (μs)	J (nm^6)	R_0 (nm)	τ_{ET} (μs)	κ_{ET} (μs^{-1})
Nd-to-Yb	0.95	10200	0.83	0.0063	160
Yb-to-Nd	9.8	49	0.34	13	0.077